Streamlining Aerodynamic CFD Analyses
Authors: Dr. Marc Ratzel, Thomas Ludescher (Altair Engineering Inc., MI, USA)
Presenter: Dr. Marc Ratzel, *Program Manager CFD*
NAFEMS World Congress 2013
June 9-12, 2013, Salzburg, Austria

Streamlining Aerodynamic CFD Analyses

by Dr. Marc Ratzel, Thomas Ludescher (Altair Engineering Inc., MI, USA)

Summary

External aerodynamic simulations using computational fluid dynamics (CFD) are well established tools in the product development process for the automotive and aerospace industries. CFD simulation technology helps engineers to understand the physical phenomena taking place in their design and provides an environment to optimize the performance with respect to certain design criteria.

In the automotive domain for example, the aerodynamic forces, e.g. lift, drag and cross force, have a strong impact on the vehicle's fuel efficiency and handling behaviour. CFD can be leveraged to analyze these forces and to determine an optimal design.

In this presentation, a vertical application to perform wind tunnel simulations of vehicles in an efficient, accurate and robust manner is discussed. An intuitive user interface streamlines the process to define parameters for meshing as well as CFD case setup. The definition of physical objects, like rotating wheels or heat exchangers, includes intelligent automation to reduce the user interaction to a minimum. Multiphysic aspects like Fluid Structure interaction (FSI) can be included as well, e.g. the deflection of a spoiler due to aerodynamic loads and its impact on the lift force of the vehicle.

A connection to a high performance computing system can be leveraged directly from the user interface to expedite the memory and compute intensive tasks such as volume meshing, solving and post-processing. Automatic report generation is embedded in the system to summarize information about the numerical model, e.g. mesh statistics or boundary conditions, as well as the aerodynamic results, e.g. lift and drag coefficient.

In general, external aerodynamic flows exhibit a transient behavior, especially for road vehicles. However, the simulations are often performed in steady state mode to reduce the computer run time and to increase the turnaround time for different designs.

In the presented vertical solution, transient CFD simulations including Detached-Eddy Simulation (DES) for turbulence modeling are performed. The core technology is Altair's general purpose CFD solver AcuSolve, which is based on the Galerkin/Least-Square (GLS) finite element method and architected for large scale problems on unstructured element topology. It allows for short computer run times while providing a high degree of accuracy due to transient modeling.

Classical aerodynamic benchmarks as well as realistic vehicles will be discussed regarding result accuracy and CPU run times. A simplified automotive rear wing spoiler is investigated regarding the structural deformation under aerodynamic loads and its impact on the lift force.

Keywords
External aerodynamics, Virtual Wind Tunnel (VWT), Fluid-Structure-Interaction (FSI)

1. Introduction

The external aerodynamics plays an important role in the development process of modern automotives. The vehicle's performance (e.g. fuel consumption), its stability (e.g. cross wind sensitivity) and the vehicle's cooling system (e.g. engine cooling) are all influenced by aerodynamic loads. Furthermore, the driver's comfort (e.g. interior cabin noise due to vortices) and the driver's visibility (e.g. performance of wipers) depend on the external flow field.

The automotive industries apply wind tunnel experiments and computational fluid dynamic (CFD) simulations to study the aerodynamic loads on their vehicles. Fast computer systems and sophisticated numerical methods allow the investigation of complex flow structures in an acceptable turnaround time. As a result, CFD simulations became more and more popular and the number of wind tunnel experiments during a vehicle's development process got reduced. Wind tunnel testing is still an essential step in the automotive industry and a combination of virtual and experimental testing will always go hand in hand.

This paper presents a vertical solution to perform external aerodynamic analyses in an efficient, robust and accurate manner. In the following second section the general workflow is presented. The third section discusses the underlying CFD technology and numerical modeling methods. The simulation results for standard automotive aerodynamic benchmarks and for realistic vehicles are presented in section four. Section five discusses the deflection of a simplified automotive rear wing using the Fluid-Structure Interaction (FSI) capabilities of the CFD solver. A summary and conclusions of the work are given in section six.

2. Workflow

This section describes the workflow of the Virtual Wind Tunnel (VWT), an environment for external aerodynamic CFD analyses. VWT simplifies the CFD case setup, contains automatic volume meshing and batch oriented post-processing.

The general workflow to perform an aerodynamic CFD analysis of a vehicle can be described in four steps

1. Model preparation (e.g. geometry cleanup or surface meshing)
2. Volume meshing
3. CFD case setup and solver run
4. Post-processing

The Virtual Wind Tunnel (VWT) combines step 2, 3 and 4 in a streamlined process, see Fig. 1. After loading a surface mesh of the vehicle into VWT, the user can adjust the dimensions of the wind tunnel, position the car, perform the CFD case setup and define the meshing parameters. Clicking the "Run" button will start the volume meshing, solving and post-processing step in sequential order on a high performance compute cluster. After finishing the run and post-processing step, the user can review the automatically generated report of the CFD analysis, including mesh statistics, setup parameters and numerical results.

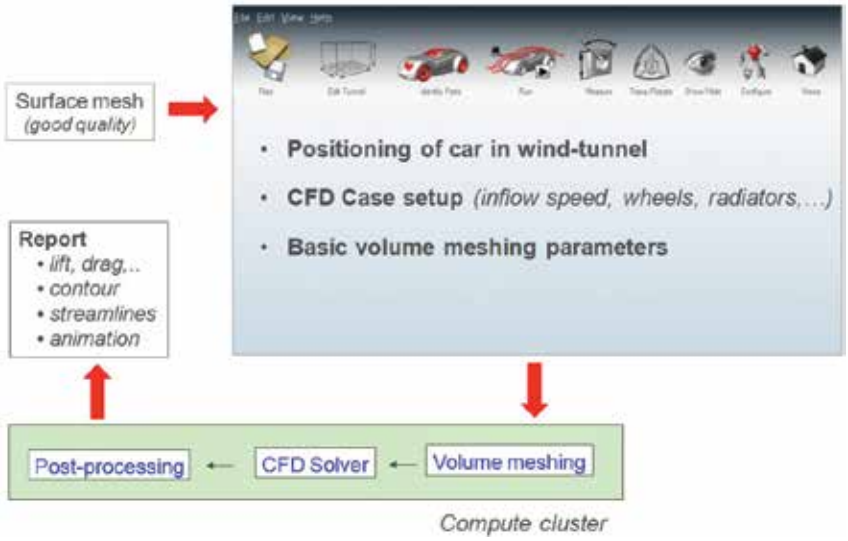

Figure 1: Workflow of the Virtual Wind Tunnel for aerodynamic CFD analyses.

During the CFD case setup, parts can be identified as body, wheel or heat exchanger and boundary layer meshing can be defined on a part basis, see Fig. 2. Depending on the part's identification, the numerical modeling differs. By default all parts are considered as body and a standard viscous wall boundary condition is applied during the CFD run.

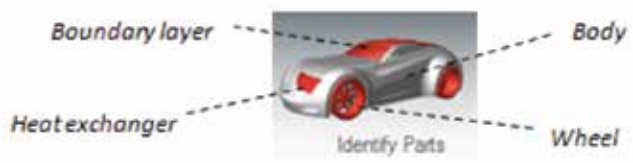

Figure 2: Utility to identify parts as body, heat exchanger or wheel.

With a simple mouse click, the user can select parts which are forming a wheel, e.g. tire and rim. All other parameters like center of rotation, axis of rotation and the rounds per minute (RPM) are computed automatically, see Fig. 3. If multiple parts are selected, an intelligent logic will group the parts into one wheel or into separate wheels. In the CFD run the rotation of each wheel is modeled by applying an individual tangential velocity. Despite the automation during wheel definition, the user has always the option to change the parameters or the grouping of the wheels if desired.

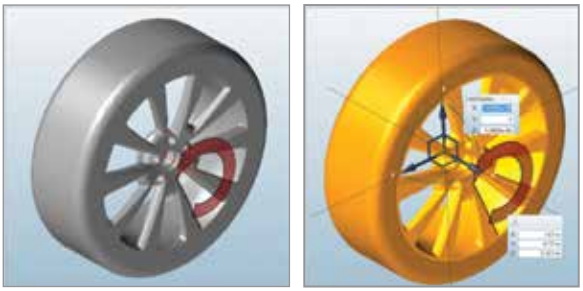

Figure 3: Parts identified as wheel, direction of rotation (left), center and axis of rotation (right).

To identify parts forming a heat exchanger, the user has to select the inflow and the outflow of each individual heat exchanger and specify the porosity parameters. The permeability direction is determined automatically, but can be modified by the user if desired. The heat exchangers are modeled as a porous media in the CFD solver run.

An accurate CFD analysis requires a boundary layer meshing technique in the vicinity of the vehicle. Growing boundary layers on all parts of the vehicle might result in a high number of elements after the volume meshing step and might require a long CPU time for the CFD analysis. In VWT, the user can select the individual parts which need to be considered for boundary layer growth during the meshing step. This helps to reduce the overall element count.

The physical run time of the transient simulation, the time increment and the frontal projected area of the vehicle are computed automatically based on the vehicle's dimension, but can be changed by the user if desired.

To define the meshing parameters the user can choose between three pre-defined sets of parameters or a user defined mesh size. An estimate for the total volume element count is displayed to inform the user. During the meshing step, several volume refinement zones around the vehicle and an adequate boundary layer are generated to resolve the flow accurately.

After the CFD run is completed an automatic report is generated in pdf format. It contains information about the CFD case setup, the dimension of the problem, aerodynamic results and animations, see Fig. 4. The report is customizable and can be adapted/enhanced easily.

Figure 4: Customizable, automatic report generation, including animations.

During run time a report can be requested as well, to check if the setup is correct and the solution is moving into the right direction. Individual post-processing of the CFD results can be performed with the post-processor included in the CFD solver suite.

3. Numerical Modeling

Performing external aerodynamic simulations of an automotive is a challenging task. The flow field is determined by a very complex geometry (e.g. engine compartment), non-stationary boundary conditions (e.g. rotating wheels and moving ground) and a turbulent flow field especially in the wake of the vehicle. To deal with those challenges, the utilized CFD solver must be accurate, scalable and robust.

In this section the CFD solver included in VWT is briefly described. Furthermore the solver's robustness and FSI capabilities are discussed.

3.1 CFD solver

The commercially available CFD solver AcuSolve is used in the above described workflow to solve the fluid dynamic equations. AcuSolve is a general purpose CFD solver applying the Galerking/Least-Square (GLS) finite element methodology to solve the Navier-Stokes equations on an unstructured mesh topology (Hughes et al. 1989, Shakib et al. 1991). The GLS approach yields high accuracy with very low requirements on mesh quality. Therefore, it is very well suited for complex automotive geometries, where the numerical grids often contain strongly distorted elements.

The flow solver is developed for parallel execution on shared and distributed memory computer systems. A hybrid parallelization methodology is used for computer architectures with a combination of distributed and shared memory. This allows quick turnaround times for typically very large aerodynamic automotive models.

AcuSolve is applicable for steady state as well as transient applications and provides second order accuracy in space and time. Sophisticated numerical diffusion operators are introduced to ensure stability while maintaining accuracy and global/local conservation. A wide variety of turbulence models are implemented in AcuSolve, including classical Reynolds-Averaged Navier-Stokes (RANS) models, Large Eddy Simulation (LES) models and hybrid RANS/LES models, often referred to as Detached Eddy Simulations (DES) models.

3.2 Robustness of the CFD solver

Due to the complex geometry of an automotive vehicle, it can be very time consuming to generate a high quality volume mesh of the fluid domain. Small gaps between two parts in the engine compartment or the tire ground connection often result in elements with high aspect ratio or a high volumetric skew value. A numerical grid of low quality can lead to divergence of the CFD solver or to inaccurate results. A refinement of the mesh can help to increase the element quality but in turn it also increases the total element count and the CPU run time.

To still ensure a quick turnaround time, the utilized CFD solver needs to be capable to deliver high quality results, even on a suboptimal mesh. Especially in the above described workflow of VWT, a robust CFD solver is an essential factor in the complete process.

To test the robustness of the CFD solver included in VWT, a simple pipe flow example is used. An initial mesh for a straight pipe is generated with a boundary layer mesh to resolve the near wall effects and a core mesh. For the core as well as the BL region tetra elements are used, resulting in highly skewed elements in the boundary region. The diameter of the pipe is then reduced at one location to one fourth of its initial

diameter, using a morphing technology, see Fig. 5. Due to the drastic reduction of the diameter, the volume mesh is highly compressed at this location and the element quality is further decreased.

Figure 5: Robustness studies on a pipe with reduced diameter.

A second mesh is generated in which the core tetra elements of the morphed mesh are remeshed to satisfy a volumetric skew of below 0.95. The tetra elements in the boundary layer mesh are maintained. Based on the second mesh a third mesh is generated in which the tetra elements in the boundary layer are replaced by standard penta elements. The reduced sections for all three grids including the max volumetric skew and the CFD results generated in AcuSolve are shown in Fig. 6.

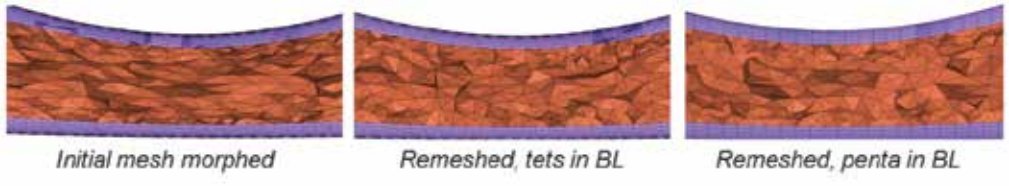

Max. vol skew	**0.9997**	**0.95** *(remeshed, tets in BL)*	**0.95** *(remeshed, penta in BL)*
Delta_p [Pa]	**2.63**	**2.63**	**2.63**
X-traction [N]	**3.13e-3**	**3.13e-3**	**3.12e-3**
Iterations	**20**	**21**	**25**

Figure 6: AcuSolve results for three grids of varying element quality.

From a standpoint of a classical finite volume scheme, the left mesh in Fig. 6 is the worst mesh and the right mesh is the best one. The pressure drop between inlet and outlet is the same for all three grids. Insignificant variations can be seen in the X-traction between the three grids and the number of iterations to reach a steady state solution is the lowest for the worst mesh.

To summarize for this example, AcuSolve converges even on highly skewed grids and is capable to produce very similar results independent of the mesh quality.

3.3 Fluid-Structure-Interaction

For the investigation of the flow around vehicles with spoilers, results in drag and lift may vary whether the spoiler components is rigid or elastic and can be deformed due to aerodynamic loads. In order to obtain an accurate result the deformation of those components should be modeled and coupled to the flow field. This could be done in a direct manner by coupling a structural code with the flow solver where the forces on the body due to the flow field are computed and passed to the structural solver which returns the deformations. Based on the structural deformation the numerical grid of the flow domain is deformed and a new flow solution is computed which generates new pressure loads.

This approach might yield long run times and high frequency oscillations might occur due to interpolation errors between non-conformal meshes on the interface between the structure and fluid domain.

In the context of this paper, it is assumed that only small displacements of the spoiler occur. Hence a different approach is used, the so called Practical-FSI (P-FSI).

The idea behind P-FSI is to use the linear equations of motions for the computation of the displacements. In order to solve those ODEs efficiently a modal analysis is carried out to project the equations into the eigenspace and thus decouple them and solve them independently. The linear finite element system of equations is given as

$$\boldsymbol{Ma + Cv + Kd = F,} \quad (1)$$

where $\boldsymbol{a}$ is the nodal acceleration, $\boldsymbol{v}$ the nodal velocity and $\boldsymbol{d}$ the nodal displacement. $\boldsymbol{M, C}$ and $\boldsymbol{K}$ are the matrices of mass, damping and stiffness respectively and $\boldsymbol{F}$ is the load vector. The matrices are constant due to linearity, i.e. no dependency on the solution (displacement $\boldsymbol{d}$). To determine the modal responses an undamped system is considered ($\boldsymbol{C}$ = 0) and together with the assumption of a harmonic solution one obtains the following eigenvalue problem

$$\boldsymbol{(K - \lambda_i M)s_i = 0,} \quad (2)$$

where λi is the i-th eigenvalue and $\boldsymbol{s_i}$ is corresponding eigenvector. Projecting the equation of motion (1) into the eigenspace yields

$$\boldsymbol{m\ddot{y} + c\dot{y} + ky = f,} \quad (3)$$

where $\boldsymbol{y}$ is the vector of amplitudes (or displacements) of the eigenmodes. In the P-FSI approach, the eigenvectors are mass-normalized

$$\boldsymbol{S^T MS = I,} \quad (4)$$

which yields to

$$\boldsymbol{m = I.} \quad (5)$$

For the remaining matrices one obtains

$$\begin{aligned} \boldsymbol{c} &= \boldsymbol{S^T CS,} \\ \boldsymbol{k} &= \boldsymbol{S^T KS} = diag(\lambda_i), \\ \boldsymbol{f} &= \boldsymbol{S^T F.} \end{aligned} \quad (6)$$

The damping matrix $\boldsymbol{C}$ is assumed to be in the described eigenspace, yielding to $\boldsymbol{c}$ being diagonal. This is a minor assumption since for most problems $\boldsymbol{C}$ is either zero or proportional to $\boldsymbol{K}$. If this is not the case it is sufficient to only take the diagonal parts of $\boldsymbol{c}$ into account.
The original variables can be reconstructed by

$$\begin{aligned} \boldsymbol{d} &= \boldsymbol{Sy,} \\ \boldsymbol{v} &= \boldsymbol{S\dot{y},} \\ \boldsymbol{a} &= \boldsymbol{S\ddot{y}.} \end{aligned} \quad (7)$$

Given this, the projected equation of motion (3) yields an uncoupled system of ordinary differential equations which can be solved independently. Furthermore, the behavior can be approximated by not using all eigenmodes but only the first n_{modes} ones. This reduces the number of equations to be solved and the memory consumption. Furthermore, it also provides some numerical stability since the higher modes are not taken into account and higher modes correspond to higher frequencies which are likely to introduce numerical instabilities. This approximation can be justified since the lower frequencies are considered as the dominant ones and the contribution of the higher frequencies is relatively small. The cutoff number n_{modes} is obviously problem specific and may vary strongly.

This approach is much faster than the direct coupling since only a small number of independent ODEs needs to be solved and this can be done within the flow solver, thus no exchange of data during runtime with a structural solver is needed. There is a multi iterative coupling (MIC) between the flow solution and the displacement solution to ensure convergence within every time step before proceeding to the next time step. The eigenmodes can be computed up front and are passed to the flow solver before starting the simulation. In order to not distort the mesh, especially the fine boundary layer mesh near the structural body, the eigenmodes can be transferred to a node set surrounding the structural body enforcing this node set to move in a similar way as the structural body, see Fig. 7.

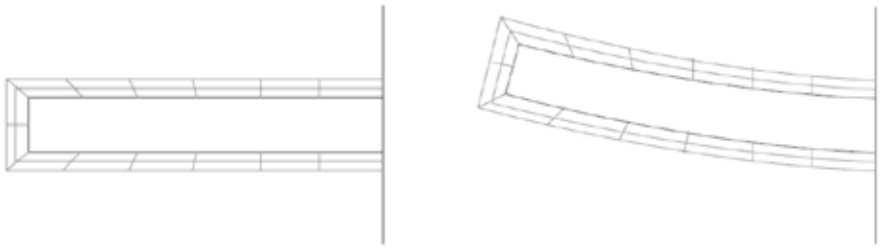

Figure 7: Moving node set to maintain boundary layer mesh during deformation.

4. Simulation results for aerodynamic automotive applications

In this section VWT is used to determine the aerodynamics of the well known Asmo model (Perzon, 2000) and the Ahmed body (Ahmed, 1984) with a rear slope of 12.5° degrees. Transient and steady state run times for two realistic car models including complex underbody and engine compartment are presented as well.

4.1 Asmo model

The Asmo model (**A**erodynamisches **S**tudien **M**odel), see Fig. 8, is a generic car model developed by the Daimler research department to investigate vehicles with a low drag coefficient and also as a neutral body for testing various CFD solvers.

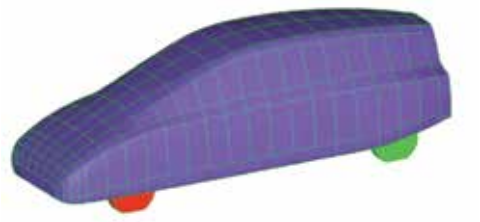

Figure 8: Asmo model, a generic low drag vehicle.

The Asmo model has a length of 0.81m, a width of 0.29m and a height of 0.27m. It is positioned in a rectangular wind tunnel with a length of 9m and a quadratic inflow surface of 1.9 x 1.9m. The distance between inflow surface and the nose of the model is 4m. The inflow speed is set to 50m/s and a DES turbulence model is used for the transient simulation with a time increment of $3 \cdot 10^{-4} s$. The numerical model contains 20Mio tetra elements, a boundary layer mesh near the body and a refinement zone in the wake.

Fig. 9 shows the pressure coefficient C_p on the symmetry plane of the model for the underbody, the roof and the rear side in comparison with two sets of experimental data. The CFD results have been averaged over several time steps to obtain a single curve. It is obvious, that the CFD results match very well the experimental data for all three cut lines. For the pressure distribution on the rear side of the model, most right plot in Fig. 9, an oscillation can be observed in the numerical results. This peak occurs at the corner where the roof meets the vertical rear side of the model. This is obviously a region of strong transient behaviour and time-averaging of the CFD results yields the shown curve.

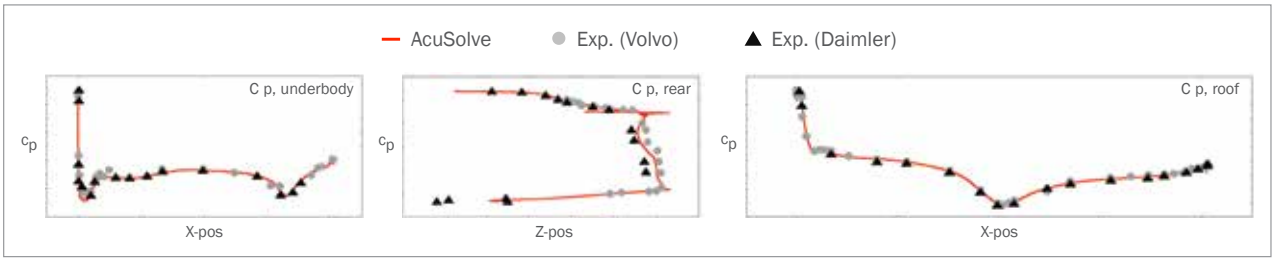

Figure 9: Pressure coefficient for the Asmo model.

The CFD run yields an averaged drag coefficient of $C_{d,\,num} = 0.164$, whereas the experimentally determined drag coefficient is $C_{d,\,exp} = 0.162$. Again, a very good match between the CFD and the experimental results can be observed.

4.2 Ahmed body

The generic Ahmed body (Ahmed, 1984), see Fig. 10, is a simplified automotive vehicle which has been used to evaluate turbulence models and CFD solvers. It is a bluff body which retains some major characteristics of an automotive, like close proximity to the ground and a sloped rear. Variations of the Ahmed body exist for different slant angles. Wind tunnel experiments show two critical angles, α=12.5° and α=30°, of the rear slope, where the time-averaged flow structures in the near wake of the body change significantly. In the context of this paper the first critical angle of α=12.5° degrees is chosen.

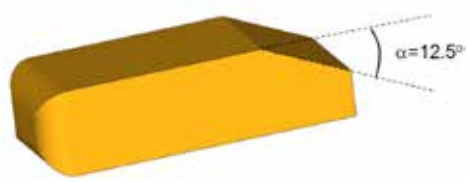

Figure 10: Ahmed body, a simplified automotive vehicle.

The body has a length of L=1044mm, a width of 389mm and a height of 288mm. It is placed in a wind tunnel with a length of 10L, a width of 2L and a height of 1.5L, where L is the length of the Ahmed body. The nose of the body is positioned 2.4L downstream of the inflow boundary and the distance between body and ground of the wind tunnel is 50mm. The inflow speed is set to 40 m/s and a DES turbulence model is used for the transient simulation with a time increment of $4 \cdot 10^{-4} s$. The numerical model contains 23Mio tetra elements, a boundary layer mesh near the body and refinement zones in the wake.

The left part of Fig. 11 shows the transient drag coefficient of the CFD run in comparison with the experimental results of $C_{D,\,exp}$=0.23. The oscillation of the drag coefficient comes from the transient behaviour of the flow field in the wake of the body. Time-averaging of the transient drag values yields a value of $C_{D,\,num}$=0.231.

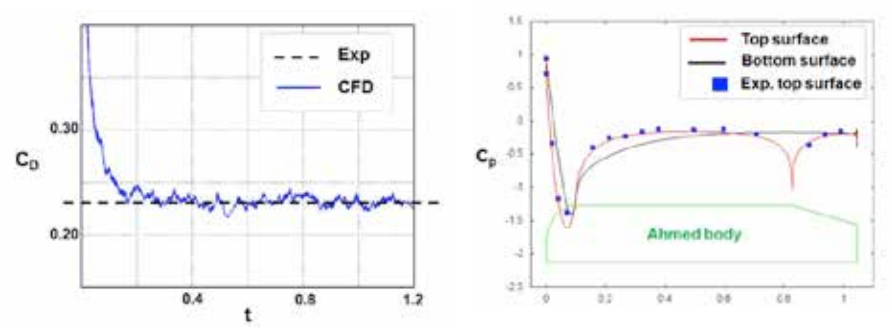

Figure 11: Comparison between CFD and exp. results, drag coefficient (left), pressure coefficient (right).

The right part of Fig. 11 shows the comparison between the numerical and experimental pressure coefficient C_p on the symmetry plane of the Ahmed body. Experimental data are only available on the top surface of the body (Bayraktar, 2001). On the bottom of the right plot in Fig. 11, the upper half of the Ahmed body's silhouette is shown. The numerical results slightly differ in the front part, where the rounded front of the body meets the straight top surface. In all other locations the correlation is very good.

To summarize, the time averaged CFD results for the drag coefficient as well as for the pressure coefficient match very well the experimental data for the Ahmed body with a slant angle of 12.5° degrees.

4.3 Realistic car model

In this section VWT is used to determine the aerodynamics of two realistic vehicles. The first model (car 1) includes a complex underbody and an engine compartment. The second model (car 2) has a flat underbody, no engine compartment and sophisticated wing-spoiler configurations to control the downforce . For both models steady state as well as transient simulations were performed

Fig. 12 shows the CPU times of the volume meshing steps as well as CFD run times. The volume meshing is performed on one processor, whereas the CFD solver runs are executed in parallel on multiple processors. The resulting drag coefficients are in good correlation with the experimental results, which cannot be shown here for confidentially reasons.

	Vol. meshing	CFD run (steady)	CFD run (transient)
Car 1	80min / 90Mio cells	3h / 192 cores	13h / 192 cores / t=1.3s
Car 2	50min / 96Mio cells	8h / 120 cores	28h / 120 cores / t=1s
	80min / 225Mio cells	20h / 120 cores	---

Figure 12: Volume meshing and CFD solver run times for two realistic automotive models.

It can be seen, that the volume meshing step is very fast, even below 1 hour for one configuration of car 2. One reason for this is that the utilized CFD solver is very forgiving regarding element quality. Therefore, the commonly required mesh optimization steps can be omitted, which shortens the meshing time drastically.

External automotive aerodynamics is by nature a transient phenomenon and can only be approximated with the stationary CFD solution. The transient simulations described in Fig. 12 are performed up to a physical time of t=1.3s for car 1, and t=1s for car 2. Both CPU run times are in an acceptable range to justify the utilization of transient CFD simulations during the automotive development process. The fast volume meshing algorithm further reduces the turnaround time for CFD results.

5. Structural deformation of a rear wing under aerodynamic loads

In this section a simplified automotive rear spoiler is placed in a wind tunnel and the effects of the structural deformations of the wing onto the lift force are investigated.

For the results presented within this paper a generic Formula One rear wing is investigated, see Fig.13.

Figure 13: Spoiler geometry and structural constraints.

Bounding boxes around the component have the dimensions $0.17\text{m} \times 0.54\text{m} \times 0.02\text{m}$ for the wing blade and $0.22\text{m} \times 0.55\text{m} \times 0.27\text{m}$ for the sides. The spoiler is placed in a rectangular wind tunnel with dimension $14\text{m} \times 5.5\text{m} \times 2.3\text{m}$ and 3m downstream of the inflow boundary. The boundary conditions are set to *wall* for the ground and the spoiler. For the inflow a velocity of $50\ m/s$ and an eddy viscosity of $10^{-4} m^2/s$ is specified. A constant pressure is specified for the outflow and the walls are set to *slip*.

For the simulation the fluid model is set to air at standard atmosphere with constant density and the transient Navier-Stokes equations with the Spallart-Allmaras turbulence model are solved.

To compute the eigenmodes of the structure for the P-FSI approach, the structural model needs to be defined. The green triangles at the bottom of the vertical plates in Fig. 13 represent the structural constraints which are no translation and no rotation in any direction, thus completely fixed. To carry out a modal analysis as described in section 3.3, the material model has to be specified. For the investigations within this paper a soft plastic material with the properties $E=3\ GPa$ (Young's modulus), $\upsilon=0.3$ (Poisson ratio) and $\varrho=3000\ kg/m^3$ (density) together with a thickness of $2mm$ is specified.

The number of surface elements on the wing is 174,000 and the total number of elements is 26Mio. The number of boundary layers for the wing is set to 20 with a first layer height of $10^{-5}m$ and a growth rate of 1.3. The ground is meshed with a boundary layer as well containing 4 layers, a first layer height of $10^{-3}m$ and a growth rate of 1.3.

As mentioned in section 3.3, the number modes is problem specific and in order to find a good balance between accuracy and efficiency a comparison between two runs with 20 and 100 eigenmodes has been carried out.

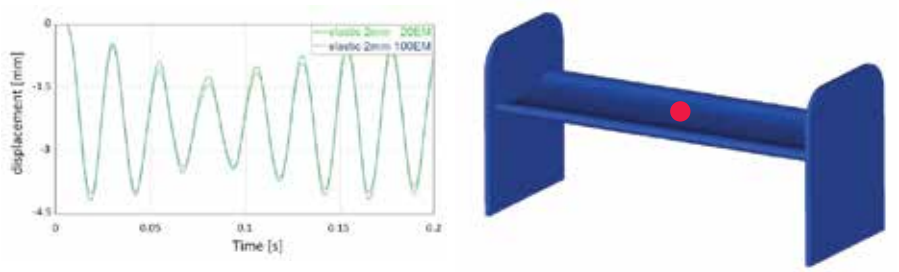

Figure 14: Displacement in z-direction for 20 and 100 eigenmodes.

Fig. 14 shows the displacement of a monitor point located in the center of the upper side of the wing (see red dot, on the right) for 20 (green) and 100 (blue) eigenmodes. It can be observed that the frequency matches quite well but the displacements are slightly smaller for the higher number of modes.

It turns out that the modes corresponding to higher frequencies affect only the vertical side boards and leave the wing blade untouched. For the purpose of this paper only the first 20 modes are considered.

Fig. 15 shows the effects on lift for a simulation of an elastic spoiler, using the above described material model, compared to a run with a rigid spoiler where no structural response is modeled.

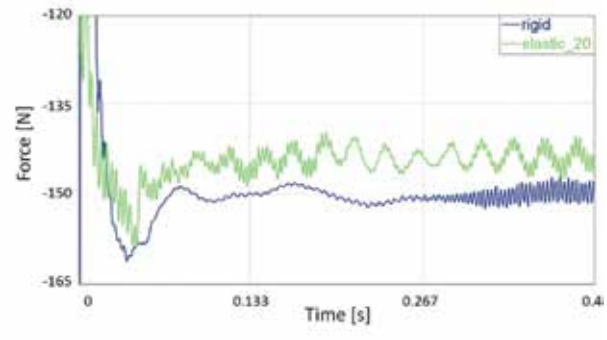

Figure 15: Lift forces for rigid and FSI run.

The structural response is clearly visible in the fluctuations of the lift force (green curve) and also the magnitude of the lift is smaller resulting in a smaller downforce.

Both simulations are transient and have a time increment of $5 \cdot 10^{-4} s$. For FSI simulations the time increment should be chosen in a manner that the highest present modal frequency as well as the flow phenomena, e.g. turbulent structures, can be resolved accurately.

The rigid case ran for 15.5h with 800 time steps on 48 cores and the FSI simulation required 30h for 1000 time steps on 60 cores. The longer run time for the FSI case is expected not only because of an additional set of equations to solve but also because of the multi iterative coupling for every time step which requires certain iterations to converge as opposed to the rigid case where no coupling is present.

The question might arise whether it is worth all the effort to include a structural response into the model. Averaging the lift forces over the last 100 time steps yields -143.92 N for the FSI case and -149.67 N for the rigid case. Thus the deviation of the FSI lift to the rigid lift is 3.8%. Based on this result, the integration of FSI capabilities into the modeling allows a more detailed analysis of the flow process and should be considered if the spoiler plays a significant role for the overall lift computation, e.g. race car domain.

Summary

In this paper a vertical solution to perform aerodynamic automotive CFD analyses in a streamlined way has been presented. The Virtual Wind Tunnel (VWT) solution consists of a “light” user interface to define the case setup, an automated volume meshing step, solver job submission and batch-oriented post-processing.

The key characteristics of VWT are accuracy, efficiency and robustness. The robustness and accuracy of the process are results of the Galerkin/Least-square (GLS) based CFD solver, allowing high quality results even on strongly distorted grids. The efficiency of the process is ensured by intelligent automation during case setup and a quick turnaround time for steady state or transient CFD simulations.

CFD simulations for the Asmo and the Ahmed body have been performed, yielding very good results for drag and pressure coefficients compared to experimental data. Two realistic car models have been studied as well, showing quick turnaround times for transient and steady state CFD simulations.

The deformation of a rear wing under aerodynamic loads has been investigated by a transient FSI simulation. A linear approach has been chosen since only small structural displacements are expected. The results show a noticeable difference in the lift force between the deformable and the non-deformable rear wing.

The Virtual Wind Tunnel (VWT) solution is a streamlines environment for pure aerodynamic investigations as well as multiphysic applications including Fluid-Structure-Interactions (FSI).

References

[1] Ahmed S.R., Ramm G., Faltin G., 1984, *Some Salient Features of the Time-Averaged Ground Vehicle*, SAE paper 840300, pp 1-31.

[2] Bayraktar I., Landman D., Baysal O., 2001, *Experimental and Computational Investigation of Ahmed Body for Ground Vehicle Aerodynamics*, SAE paper 2001-01-2742.

[3] Perzon S., Davidson L., 2000 *On Transient Modeling of the Flow Around vehicles Using the Reynolds Equations*, ACFD Beijing Oct 17-20, pp 720-727.

[4] Hughes T., Franca L., Hulbert G., 1989 *A new finite element formulation for computational fluid dynamics. VIII. The Galerkin/Least-Square method for advective-diffusive equations.* Computer Methods in Applied Mechanics Engineering, 73, pp 173-189.

[5] Shakib F., Hughes T., Johan Z., 1991, *A new finite elements formulation for computational fluid dynamics.X. The compressible Euler and Navier-Stokes equations.* Computer Methods in Applied Mechanics Engineering, 89, pp 141-219.